Research Paper

Low Molecular Weight Heparin-Coated and Dendrimer-Based Core-Shell Nanoplatform with Enhanced Immune Activation and Multiple Anti-Metastatic Effects for Melanoma Treatment

Chunyu Xia, Sheng Yin, Shanshan Xu, Guangyao Ran, Miao Deng, Ling Mei, Xian Tang, Jingdong Rao, Man Li, Zhirong Zhang, Qin He✉

Key Laboratory of Drug Targeting and Drug Delivery Systems, West China School of Pharmacy, Sichuan University, No. 17, Block 3, Southern Renmin Road, Chengdu 610041, China.

✉ Corresponding author: Fax/Tel: 86 28 85502532; Qin He: qinhe@scu.edu.cn

Abstract

High-efficiency treatment for tumor is not easy to achieve owing to the existence of metastasis, which remains the arch-criminal of most tumor deaths. Conventional chemotherapy exhibits insufficient inhibitory efficiency on tumor metastasis and more powerful strategies to conquer metastatic tumors are urgently needed. In this study, a rational chemoimmunotherapy strategy was adopted to treat highly aggressive melanoma based on a newly developed multifunctional nanoplatform. Firstly, immunoadjuvant cytosine-phosphate-guanine oligonucleotides (CpG ODNs) were used to boost the doxorubicin (DOX)-elicited immune responses, which synergistically suppressed tumor growth and metastasis. And the anti-metastatic low molecular weight heparin (LMWH) was also integrated, thus multiple anti-metastatic effects to against tumor metastasis were achieved.

Methods: G4 PAMAM was serving as the main support to conjugate DOX by pH-sensitive hydrazone bond (PPD) and the synthesized conjugates were confirmed by ^{1}H-NMR spectra, IR spectra and HRMS. Immunoadjuvant CpG ODNs were loaded by electrostatic adsorption to formulate PPD/CpG. After the coating of anti-metastatic LMWH, the designed LMWH/PPD/CpG was fabricated and characterized. The platelets-related and platelets-unrelated anti-metastatic mechanisms were investigated on B16F10 melanoma cells. The capacity of DOX to elicit immunogenic cell death (ICD) on B16F10 melanoma cells was examined by flow cytometry, laser scanning confocal microscope and immunohistochemical staining. Then the immune activation effects, anti-tumor and anti-metastatic efficacy of LMWH/PPD/CpG were evaluated on a B16F10 melanoma xenograft model.

Results: DOX elicited tumor-specific immune responses by ICD, and the immunological effects could be further promoted by CpG ODNs, exhibiting enhanced maturation of dendritic cells (DCs) and increased level of cytolytic T lymphocytes (CTLs) *in vivo*. Owing to the coating of LMWH, the platelets-induced epithelial-mesenchymal-like transition of tumor cells was hindered and the actin cytoskeletal arrangement of tumor cells was affected, thus the migration ability of tumor cells was further inhibited. This multifunctional nanoplatform showed enhanced treatment efficiency on melanoma primary tumor and pulmonary metastasis.

Conclusion: The immune activation and multiple anti-metastatic effects of LMWH/PPD/CpG establish a novel therapeutic strategy for melanoma. This anti-metastatic nanoplatform could be broadly applied for the co-delivery of other nucleic acids and chemotherapeutic drugs to treat highly aggressive tumors.

Key words: immunogenic cell death, PAMAM, low molecular weight heparin, multiple anti-metastatic, pH sensitive

Introduction

Studies indicate that > 90% of mortality from cancer is attributable to metastasis, but not the primary tumors [1]. Although chemotherapy is widely used in the treatment for many kinds of cancers, conventional chemotherapy strategies always exhibit insufficient inhibition on tumor metastasis [2,

3]. And due to the nonspecific distribution of many chemotherapeutic drugs, although researchers have developed various nanocarriers to realize the targeted delivery of chemotherapeutic drugs [4], the drug concentrations in tumor region are still limited. Multiple administrations unavoidably lead to high risks of systemic toxicity and multiple drug resistance [5]. In order to improve the anti-tumor outcome, superior strategies which could optimize the treatment efficiency of chemotherapy and provide more powerful force to suppress tumor metastasis are urgently needed. Tumor immunotherapy has progressed rapidly these days and shown many encouraging results [6, 7]. Researches have indicated that appropriate immunotherapy has the unique ability to specifically eradicate primary tumor and control metastasis without damaging normal cells [8]. Thus, the immunotherapy-involved combined therapy might be a more attractive approach to conquer tumor, which could reduce the dosage of chemotherapeutic drugs to alleviate the potential side effects and achieve more effective suppression on tumor growth and metastasis.

The relevance between chemotherapy and immunotherapy has gained more and more attention in recent years [9]. Accumulating evidences suggest that chemotherapy-elicited immune responses significantly contribute to the overall anti-tumor activity and the past few years have witnessed the emergence of an important concept of ICD (immunogenic cell death) [10, 11]. ICD is a cell death modality elicited by specific chemotherapy or radiotherapy, and the dying tumor cells could act as anticancer vaccines allowing the immune system to contribute through a "bystander effect" to eradicate chemotherapy- resistant tumor cells and tumor stem cells [12]. DOX, one of the anthracyclines, which has been demonstrated to possess the ability of eliciting ICD on melanoma, breast cancer or colon cancer [13, 14]. DOX-elicited ICD could promote the exposure of calreticulin (CRT), and the engulfment of dying cells or the presentation of tumor antigens is also facilitated, leading to immune responses with elevated levels of IFN-γ and tumor-specific CTLs [15]. Considering that the immunological effects elicited by DOX are restricted, potent immunoadjuvants are emerging as good candidates to boost the DOX-elicited immune responses. CpG ODNs, a type of immunostimulatory nucleic acid, which can be recognized by the toll-like receptor 9 (TLR9) expressed on the immune cells (such as pDCs and B cells) and are already used in clinical trials for melanoma. It can activate the host defense mechanisms by mitogen-activated protein kinases (MAPKs) and MyD88-dependent nuclear factor-κB (NF-κB) signaling pathways, initiating a cascade of innate and adaptive immune responses [16-18]. Several studies also indicate that CpG ODNs can markedly improve tumor response to chemotherapy and radiotherapy, indicating the possibility of using CpG ODNs to strengthen the DOX-elicited immune responses.

The activated immune system could enhance the inhibitory efficiency on tumor metastasis. However, tumor metastasis is a series of complicated multistep cell-biological processes termed invasion-metastasis cascade and affected by many factors *in vivo* [19-21]. Plenty of researches have demonstrated that platelets could adhere to tumor cells and promote metastasis by resulting platelets-induced EMT-like transformation of tumor cells, preventing tumor cells from death in the circulation and assisting them to pass through the vascular endothelium [22, 23]. Thus, blocking the interactions of platelets on tumor cells could further suppress tumor metastasis. Notably, our previous studies have demonstrated the favorable anti-metastatic effects of LMWH [24]. It could not only inhibit the platelets-induced EMT-like transformation of tumor cells, but also exhibit the anti-metastatic effects by affecting the actin cytoskeletal arrangement of tumor cells. Superior to artificial materials, LMWH is a natural, biodegradable and non-immunogenic polysaccharide, which arouses our interest to use LMWH as a part of the carriers for drug delivery.

Therefore, we designed a LMWH-coated anti-metastatic nanoplatform and adopted a chemoimmunotherapy strategy by integrating the therapeutic efficacy of DOX and CpG ODNs rationally to treat metastatic melanoma. With the aim of delivering DOX and CpG ODNs simultaneously, cationic polyamido-amine dendrimer (amino- terminated PAMAM) emerged as a promising vehicle. A newly developed method to conjugate DOX on the amino-terminated PAMAM dendrimer by pH-sensitive hydrazone bond (PPD) was introduced in this article. We also confirmed that the synthesized PPD conjugates had favorable properties to load nucleic acids. Besides, the coating of negative-charged LMWH not only provided the anti-metastatic effects, but also shielded the positive charge of PPD/CpG, which could reduce the clearance by the reticuloendothelial system (RES) for better tumor accumulation and reduce the potential toxicity of cationic nanoparticles. Many researches indicated that the LMWH or heparin coated on the surface of cationic nanoparticles could be degraded by heparanase, which was over-expressed in many tumors, including melanoma [25, 26]. Finally, the rational combination of chemotherapy and immunotherapy based on this multifunctional core-shell nanoplatform showed enhanced treatment efficiency on melanoma primary tumor and pulmonary metastasis.
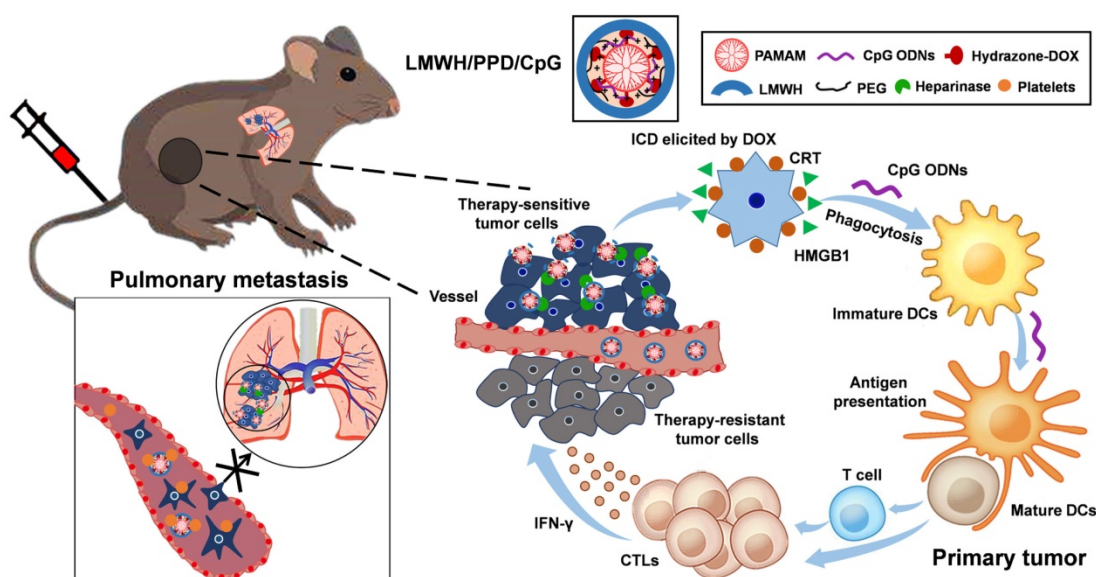
Figure 1. Schematic illustration of LMWH/PPD/CpG to inhibit melanoma primary tumor and pulmonary metastasis.

Methods

Synthesis and characterizations of PEG-PAMAM conjugates

PEG-PAMAM conjugates were synthesized by conjugating the primary amino groups of G4 PAMAM dendrimer with mPEG-SVA [27]. Briefly, mPEG-SVA (14.10 mg, 2.82 μm) were added to the solution of PAMAM dendrimer (20.00 mg, 1.41 μm) in 2 mL of 0.2 M phosphate buffer solution (pH 8.0). The reaction mixture was stirred in the presence of N_2 for 24 h, then the solution was transferred into a dialysis membrane (molecular weight cutoff = 8000-12000 Da) and dialyzed against water to remove the excess unbound PEG. The products were retrieved by freeze drying and white solids were obtained. The successful synthesis of PEG-PAMAM conjugates was confirmed by ^{1}H-NMR spectra, IR spectra and HRMS.

Synthesis and characterizations of PEG-PAMAM-MA conjugates

PEG-PAMAM-MA conjugates were synthesized by Michael addition [28, 29]. Firstly, PEG-PAMAM (25.56 mg) was dissolved in 2 mL of anhydrous methanol and stirred for half an hour, then cooled on an ice-water bath. Methyl acrylate (MA) (3.05 μL) was then added to the magnetic stirring solution within the flask under N_2. After ice-water bath was removed, the round-bottom flask was sealed and the reaction mixture was stirred at 25 °C for 48 h. After reaction, methanol was removed in vacuum. The successful synthesis of PEG-PAMAM-MA conjugates was confirmed by ^{1}H-NMR spectra, IR spectra and HRMS.

Synthesis and characterizations of PEG-PAMAM-MA-hydrazine conjugates

PEG-PAMAM-MA conjugates were subjected to the reaction with hydrazine. Firstly, PEG-PAMAM-MA (28.47 mg) conjugates was dissolved in 2 mL of anhydrous methanol, then 100 μL of hydrazine (an excess amount) was added to the solution and kept continuous stirring in the presence of N_2 at 40 °C for 48 h. After the reaction, the solution was dialyzed using a dialysis membrane (molecular weight cutoff = 8000-12000 Da) and the white solids were obtained by freeze drying. The successful synthesis of PEG-PAMAM-hydrazine conjugates was confirmed by ^{1}H-NMR spectra, IR spectra and HRMS.

Synthesis and characterizations of PEG-PAMAM-DOX conjugates (PPD)

DOX was conjugated to the hydrazine moiety via hydrazone bond. PEG-PAMAM-MA-hydrazine conjugates (25.00 mg) were dissolved in 1 mL DMSO, then 13.50 mg DOX in 1 mL DMSO was added. The mixture was allowed to react in the presence of N_2 in darkness at 40 °C for 48 h. After the reaction, the solution was transferred into a dialysis membrane (molecular weight cutoff = 8000-12000 Da) to remove the unbound DOX and DMSO. Then the red solid was attained by freeze drying. The successful synthesis of PPD conjugates was confirmed by ^{1}H-NMR spectra, IR spectra and HRMS. Then, the content of DOX in PPD conjugates was measured by spectrofluoro-photometer (Shimadzu RF-6000, Japan). The *in vitro* DOX release experiment was performed by using the dialysis method at different pH values (7.4, 6.8 and 5.0).

Preparations and characterizations of PPD/CpG and LMWH/PPD/CpG

Firstly, CpG ODNs solution was dropped into an equal volume of PPD solution and quickly mixed by vortex, followed by incubation at room temperature for 30 min to form PPD/CpG. The adsorption ability of PPD to CpG ODNs was evaluated by agarose gel electrophoresis at different mass ratios of 0: 1, 0.25: 1, 0.5: 1, 1: 1, 2: 1, 4: 1, 8: 1, 12: 1. For the preparation of LMWH/PPD/CpG, the amount of LMWH on the surface was also screened by agarose gel electrophoresis. To attach the negative-charged LMWH on the surface of PPD/CpG, LMWH solution (mass ratio to PPD: 0.1: 1-1: 1) were added dropwise into the PPD/CpG solution, followed by quickly mixed by vortex and incubation at room temperature for 2 h.

FRET (fluorescence resonance energy transfer) experiment was further carried out to confirm the successful coating of LMWH on the surface of PPD/CpG. DOX was used as the fluorescence donor and Cy5 was used as the fluorescence acceptor [30]. The Cy5-LMWH conjugates were obtained by the amidation reaction between the amino group of Cy5 and the carboxyl group of LMWH in a mixed solvent of DMF and formamide (19: 8). Then PPD/CpG at the same DOX concentration of 10 µg/mL was coated with Cy5-LMWH at different concentrations to form nanoparticles with Cy5/DOX mass ratios of 1: 2 and 1: 1. Cy5-LMWH and PPD/CpG were set as controls, with Cy5/DOX mass ratios of 2: 0 and 0: 2, respectively. The emission spectra were recorded by spectrofluorophotometer (Shimadzu RF-6000, Japan) and 450 nm was set as the excitation wavelength.

Subsequently, the size distributions and zeta potentials of PPD, PPD/CpG and LMWH/PPD/CpG were measured by dynamic light scattering (DLS) method using Malvern Zetasizer Nano ZS90 (Malvern Instruments Ltd., U.K.). And the morphology of these nanoparticles was observed using transmission electron microscope (Hitachi H-600, Japan).

The serum stability assay of LMWH/PPD/CpG in 50 % fetal bovine serum (FBS) was performed and the light transmittances at different time points (0 h, 1 h, 2 h, 4 h, 8 h, 12 h and 24 h) were determined by using Varioskan Flash Multimode Reader (Thermofisher, USA).

Inhibitory effects on cell migration and invasion

The inhibitory effects of different formulations on the migration and invasion ability of B16F10 cells was investigated by wound healing assay and transwell assay. For the wound healing assay, B16F10 cells were seeded into 6-well plates and when cells grown to near confluence, the wounds were scratched by a sterile pipette tip. Subsequently, the cells were treated with HEPES (HEPES buffer), free LMWH, PPD, free DOX, or LMWH/PPD and incubated for 24 h. Images were obtained at 0 h and 24 h using a microscope (Leica DMi1, Germany). For transwell invasion assay, B16F10 cells were suspended in 0.5% serum medium and plated to the top chamber of transwell (24-well insert, pore size, 8 µm, Coring, USA) precoated with Matrigel (BD, Bioscience). Then 600 µL of culture medium containing 20% FBS was used as a chemoattractant. After treatment with HEPES, free LMWH, PPD, free DOX or LMWH/PPD, the cells that did not invade were removed with a cotton swab, then the invaded cells were stained with crystal violet. Finally, the bottom of the chamber was photographed and the crystal violet was eluted by 33% acetic acid solution to measure the absorbance at 570 nm by using Varioskan Flash Multimode Reader (Thermofisher, USA).

Laser scanning confocal microscope of actin cytoskeleton

B16F10 cells were seeded into 6-well plates at a density of 1×10^5 cells/well and incubated for 24 h. After treatment with HEPES, free LMWH, PPD, free DOX or LMWH/PPD for 12 h, the cells were fixed by 4% paraformaldehyde and incubated with FBS (1% in PBS) to block aspecific labeling. Then, the cells were incubated with ActinRed for 20 min at room temperature and the nuclei were stained with DAPI. Finally, the actin cytoskeleton was visualized under laser scanning confocal microscope (LSM 800, Zeiss, Germany).

Interactions of platelets on B16F10 cells

Whole blood was collected from mice orbit and fresh platelets were collected by centrifugation. Briefly, B16F10 cells were seeded into 6-well plates and cultured overnight. Equal amount of prepared platelets was added into each well and cells were incubated with HEPES, free LMWH, PPD, free DOX, or LMWH/PPD, respectively. A negative control group without platelets was also set. And microscope (Leica DMi1, Germany) was used to observe the cell morphology at 24 h.

Western blot of E-cadherin and N-cadherin

E-cadherin protein and N-cadherin protein levels were evaluated by western blot. After treatment with HEPES, HEPES + platelets, free DOX + platelets, free LMWH + platelets, PPD + platelets or LMWH/ PPD + platelets for 24 h, B16F10 cells were harvested and the proteins were collected. Equal amount of total protein was loaded onto SDS-PAGE gels for separation. The polyvinylidene difluoride (PVDF) membranes were incubated with the specific primary

antibodies, washed with TBST solution (TBS with 0.05% Tween-20) and incubated with HRP-labeled secondary antibodies. Finally, the protein levels were detected with the Immobilon Western HRP Substrate (Millipore, WBKLS0500) on Bio-Rad ChemiDoc MP system (Bio-Rad Laboratories, USA).

In vivo imaging and tissue distribution

B16F10 tumor-bearing mice model (C57 mice, 5−8 weeks, 18−22g) was established by injecting B16F10 cells into the right flanks of mice at a density of 1×10^6 cells/flank in ice-cold PBS. *In vivo* imaging and biodistribution experiments were performed on day 13. To investigate the delivery ability of nucleic acid, mice were intravenously administered with HEPES, free DOX+Cy5-DNA, PPD/Cy5-DNA or LMWH/PPD/Cy5-DNA at a dose of 2 mg·Kg^{-1} Cy5-DNA. And the fluorescence imaging was performed with IVIS Spectrum (Caliper, Hopkington, MA, USA) at predetermined time points. Subsequently, the hearts, livers, spleens, lungs, kidneys, and tumors were collected and imaged. Tumors were sliced via freezing microtome section and stained with DAPI to evaluate the distribution of different formulations by using laser scanning confocal microscope (LSM 800, Zeiss, Germany).

Moreover, to further evaluate the accumulation of carriers, fluorescent probe Cy7 was conjugated on PPD by amidation reaction. Then, mice were intravenously injected with HEPES, PPD-Cy7, or LMWH/PPD-Cy7 at a dose of 2 mg·Kg^{-1} Cy7. The fluorescence imaging was performed at predetermined time points.

Effects of DOX on CRT exposure and HMGB1 release

Firstly, we detected the capacity of DOX to induce CRT exposure on B16F10 cells by laser scanning confocal microscope (LSM 800, Zeiss, Germany) and flow cytometry (Cytomics FC 500, Beckman Coulter, USA). B16F10 cells were seeded into 6-well plates at a density of 1×10^5 cells/well and cultured for another 24 h. Then, B16F10 cells were treated with free DOX, PPD or LMWH/PPD at an equal DOX concentration of 3 μM. Four hours later, the cells were incubated with primary anti-CRT antibody for 2 h and then incubated with secondary FITC antibody for 30 min. Subsequently, the photos were captured under laser scanning confocal microscope. Additionally, flow cytometry assay was performed, and the exposed CRT was detected by gating on PI-negative cells. Besides, high-mobility group box 1 protein (HMGB1) release was another signal for ICD. The CRT exposure and HMGB1 release induced by DOX were assessed by immunohisto-

chemical staining *in vivo*. B16F10 xenograft-bearing mice model was established and mice with an average tumor volume of 50-100 mm^3 were divided into 4 groups randomly: HEPES group, free DOX group, PPD group and LMWH/PPD group. Mice were intravenously injected every three days for three times. The tumor tissues were obtained and immuno-histochemical staining with anti-CRT antibody and anti-HMGB1 antibody were conducted.

In vivo immune status after different treatments

B16F10 xenograft-bearing mice with an average tumor volume of 50-100 mm^3 were divided into 6 groups randomly: HEPES group, free LMWH group, PPD group, PPD/CpG group, free DOX+CpG group and LMWH/PPD/CpG group. After treatments of every three days for three times, mice draining lymph nodes and tumors were harvested. The lymph nodes were ground and passed through 70 μm cell strainers to form single-cell suspensions. Then cells were double-stained with anti-CD11c-PE and anti-CD40-FITC, anti-CD80-FITC or anti-CD86-FITC. In addition, mice tumors were incubated with collagenase I for 1 h, then ground and filtered through the nylon mesh filters. For the detection of CD3$^+$CD4$^+$ T cells or CD3$^+$CD8$^+$ T cells, the obtained suspensions were stained with anti-CD3e-PE and anti-CD4-FITC or anti-CD8a-FITC. T$_{reg}$ cells in the tumor regions were double- stained with anti-Foxp3-PE and anti-CD4-FITC. Finally, the stained lymph nodes cells and tumor cells were analyzed by flow cytometry (Cytomics FC 500, Beckman Coulter, USA). For the detection of IFN-γ levels, the serum samples of each group were obtained after treatments. And the levels of IFN-γ were detected using specific ELISA kit following the manufacturer's instructions.

In vivo anti-tumor efficacy

B16F10 tumor-bearing mice model was established by injecting B16F10 cells into the right flanks of mice at a density of 1×10^6 cells/flank in ice-cold PBS. Then, mice with an average tumor volume of 50-100 mm^3 were randomly divided into 6 groups, and the treatments were begun on day 5. Mice were intravenously injected with HEPES, PPD, PPD/CpG, free DOX+CpG or LMWH/PPD/CpG (at an equal dose of 3 mg·Kg^{-1} DOX, 0.375 mg·Kg^{-1} CpG ODNs) every three days for three times. And free LMWH group was administered with equivalent amount of LMWH in LMWH/PPD/CpG every two days for five times. Tumor volumes and mice weight changes were measured every other day. On day 15, tumor tissues were obtained from the euthanized mice and processed for H&E staining and immunohistochemical staining.

In vivo anti-metastatic efficacy

As for anti-metastatic study, 1×10^6 B16F10 cells were inoculated into the right flanks of mice subcutaneously on the first day. Two days later, mice were injected with a total of 2×10^5 B16F10 cells via tail vein. Then mice were divided into 6 groups randomly on day 6 and administered with HEPES, PPD, PPD/CpG, free DOX+CpG or LMWH/PPD/CpG (at an equal dose of 2.5 mg·Kg^{-1} DOX, 0.3125 mg·Kg^{-1} CpG ODNs) every three days for three times. And free LMWH group was administered with equivalent amount of LMWH in LMWH/PPD/CpG every two days for five times. At the same time, the weight changes of mice were monitored. On day 21, lung tissues were obtained and the macroscopic nodules on the whole surface were counted. Then, the organs were subjected to H&E staining.

Statistical analysis

All the data were presented as mean ± standard deviation unless otherwise stated. Statistical comparisons were performed by Student's t-test for two groups and one-way ANOVA for multiple groups. And p value < 0.05 was considered as the threshold of significant difference.

Results and Discussion

Synthesis and characterizations of PPD

As described in Figure 2A, PEG-PAMAM-DOX conjugates (PPD) were successfully synthesized using this synthetic method. All compounds synthesized were confirmed by ^{1}H-NMR spectra, IR spectra and HRMS (Supplementary Material, Figure S1−S3). The content of DOX on PPD conjugates was 13.08% as measured by spectrofluorophotometer. The DOX release experiment was performed in phosphate buffer solutions with different pH values and the results were shown in Figure 2B. PPD conjugates released approximately 10% of the total DOX over 72 h at pH 7.4. And after incubation at pH 6.8, it eleased about 25% of the total DOX. Then PPD conjugates incubated at pH 5.0 showed the highest accumulative release, which was about 60% over 72 h. These results suggested that DOX was released from PPD in a pH-sensitive way. The particle size of PPD determined by DLS was about 35 ± 4.2 nm and TEM exhibited the spheroid morphology of PPD (Figure 2C). The zeta potential of PPD was about +31.2 ± 3.2 mV, which should be mainly due to the primary amino groups on the surface. The obvious positive charge of PPD provided the possibility to carry nucleic acid drugs.

Preparations and characterizations of PPD/CpG and LMWH/PPD/CpG

PPD/CpG nanoparticles were prepared by electrostatic adsorption and the DNA condensation ability of PPD at different mass ratios was assessed by agarose gel electrophoresis. As shown in Figure 2D, when the mass ratio of PPD to CpG ODNs was above 8: 1, CpG ODNs could be condensed completely, so the mass ratio of PPD to CpG ODNs should be over the threshold of 8: 1. As for LMWH/PPD/CpG, agarose gel electrophoresis was also used to determine the optimal amount of LMWH. As shown in Figure 2E, the formulations were prepared at different mass ratios of LMWH to PPD from 0.1: 1-1: 1. When the mass ratio was over 0.6: 1, the free CpG ODNs band became increasingly obvious, which could be due to the replacement effect of LMWH. Therefore, with the aim of delivering CpG ODNs and DOX simultaneously, the mass ratio of LMWH to PPD should be not over 0.6: 1. Subsequently**,** FRET experiment was further utilized to confirm the successful coating of LMWH. FRET is an effective tool to explore the interaction between nanoparticles with internal or external stimulus by detecting the fluorescence change of both donor and acceptor [31-33]. As shown in Figure 2F, strong fluorescence from PPD/CpG (DOX, 594 nm) and low emission from Cy5-LMWH (Cy5, 662 nm) were exhibited, which suggested a profound FRET effect between the donor and acceptor. Notably, fluorescence intensity of the donor (DOX) gradually declined with the increase of Cy5-LMWH, while the fluorescence intensity of the acceptor (Cy5) strongly increased. This phenomenon reflected the FRET effect between Cy5 and DOX, indicating the successful coating of LMWH on the surface of PPD/CpG.

DLS showed that the particle size of LMWH/PPD/CpG was about 25 ± 3.5 nm and TEM revealed the spheroid morphology of LMWH/PPD/CpG (Figure 2G). The zeta potential of LMWH/PPD/CpG was about -29.4 ± 3.6 mV and the charge reversal should be due to the fixation of LMWH on the surface of PPD/CpG.

Turbidity variation was used to evaluate the aggregation behavior of LMWH/PPD/CpG in 50% fetal bovine serum (FBS). The light transmittances were always over 90%, which suggested that LMWH/PPD/CpG was stable when incubated with FBS (Figure S4).

It has been reported that cationic delivery vectors could cause cell lysis and hemoglobin release [34]. Therefore, one of the benefits of LMWH coating was to shield the positive charge of delivery vectors and thus increase the safety. Hemolysis assay was conducted to evaluate the hemolysis activities of PP

and LMWH/PP. As shown in Figure 2H, the results showed that LMWH/PP had no obvious influence on red blood cells, and the hemolysis rate of LMWH/PP was consistently lower than 5% when the concentration of PP altered from 5 to 300 μg/mL. Hemolysis rate less than 5% was regarded as nontoxic [35]. In comparison, the hemolysis rate of PP was over 5% when the concentration of PP reached to 150 μg/mL. Photo images of plastic pipes containing red blood cells after cultured with PP and LMWH/PP at various concentrations were shown in Figure S5. The micrographs revealed that the structure of red cell membrane had little change after incubated with LMWH/PP, but obvious aggregation of red blood cells and the release of hemoglobin after exposure to PP were observed (Figure 2I). All these results showed that LMWH/PP was safer than PP in this regard.

Celluar uptake assay

In vitro cellular uptake assay was conducted by laser scanning confocal microscope and the results were shown in Figure S6. After 2 h of incubation, strong red fluorescence was observed in PPD group, indicating the uptake of PPD. And red fluorescence was also observed in LMWH/PPD group, which was weaker than PPD group. This probably because that PPD was highly positive-charged (+31.2 ± 3.2 mV), which made it easily be uptake by B16F10 cells. In comparison, the zeta potential of LMWH/PPD was obviously reduced after the coating of LMWH, so the cellular uptake was reduced.

Cytotoxicity assay

Firstly, MTT assay was conducted to estimate the toxicity of PP and LMWH/PP on B16F10 cells. As shown in Figure S7A, the cell viability presented obvious difference between PP group and LMWH/PP group. When cells were treated with PP at a PAMAM concentration of 0.1 μM, the cell viability rate decreased to about 60%, while LMWH/PP group exhibited a cell viability rate of over 75%. When PAMAM concentration reached 75 μM, the viability rate of PP-treated cells was about 10%, which was much lower than that of LMWH/PP group. These data indicated that the coating of LMWH decreased the cytotoxicity of cationic nanoparticles.

Subsequently, the cytotoxicity of DOX-loaded nanoparticles on B16F10 cells was also investigated. As the data shown in Figure S7B, PPD exhibited lower cytotoxicity when compared with free DOX, mainly because DOX was a small molecule which could easily cross the cell membrane and instantly affect cell growth without drug release process [35], while PPD showed a sustained-release effect of DOX. Besides, there was no obvious difference of cell viability

between PPD group and PPD/CpG group, suggesting that CpG ODNs has no evident cytotoxic effect on B16F10 cells among the tested concentration range. In addition, LMWH/PPD/CpG showed lower cytotoxicity than PPD and PPD/CpG because positively-charged PPD and PPD/CpG could easily cross cell membrane.

Inhibitory effects on cell migration and invasion

The migration and invasion ability of tumor cells are directly related to their metastasis [36]. Therefore, wound healing assay and transwell assay were conducted to evaluate the regulatory effects of different formulations on the migration and invasion ability of B16F10 cells. In the wound healing assay, HEPES-treated B16F10 cells migrated rapidly into the scratch and filled it nearly completely in 24 h (Figure 3A). However, the cell migration ability was inhibited to different extents after incubated with free LMWH, PPD, free DOX, or LMWH/PPD. The calculated wound healing rate of free LMWH group significantly declined (54.59 ± 4.96%) when compared with HEPES-treated group (80.44 ± 2.77%), indicating that LMWH could decrease the motility of B16F10 cells. PPD and free DOX group also exhibited reduced wound healing rates, perhaps owing to the cytotoxic effects of DOX. Notably, LMWH/PPD/ CpG showed the lowest wound healing rate (19.10 ± 2.12%), which might be due to the combined effects of DOX and LMWH.

In addition, the transwell assay was conducted and the results were shown in Figure 3B. The image indicated that there were many B16F10 cells invaded into the lower chamber of the transwell in HEPES-treated group, which suggested that B16F10 cells were very aggressive. The number of B16F10 cells that penetrated the matrigel-coated membrane was significantly reduced in free LMWH-treated group and the relative invasion rate was 71.61 ± 2.91%, which might be owing to the inhibitory ability of LMWH. Due to the inhibitory effects of DOX on cell viability, the number of invaded cells also decreased in PPD group and free DOX group. When compared with other groups, the number of B16F10 cells invaded into the lower layer in LMWH/PPD/CpG group was significantly decreased (with a relative invasion rate of 29.22 ± 4.46%), which could be due to the synergistic effects of DOX and LMWH.

Laser scanning confocal microscope of actin cytoskeleton

The "transformed tumor cell phenotype" based on specific cytoskeletal rearrangement is important to the efficient adhesion and migration of tumor cells

[37]. The possible effects of LMWH and LMWH/PPD on the actin cytoskeletal arrangement of B16F10 cells were investigated in our experiments. And rhodamine conjugated phalloidin was used for F-actin staining [38]. As shown in Figure 3C, HEPES-treated B16F10 cells exhibited the wide spread of F-actin, then the cells were stretched by the tensile forces of actin stress fibers, facilitating the invasion and metastasis of B16F10 cells [39]. PPD group and free DOX group could influence cell viability due to the cytotoxicity of DOX while exhibited negligible inhibition on the spread of F-actin, and the cells remained an invasive phenotype like the cells treated with HEPES. Notably, the actin cytoskeleton was disorganized when cells were treated with free LMWH or LMWH/PPD, as indicated by the smoother morphology of cells compared with cells in HEPES-treated group. This might be one of the anti-metastatic mechanisms of LMWH.

Interaction of platelets on B16F10 cells

It has been reported that platelets-derived TGF-β and direct platelets-tumor cells contact could synergistically activate the TGF-β/Smad and NF-κB pathways in tumor cells, resulting in their transition to an invasive mesenchymal-like phenotype and enhanced tumor metastasis [22]. Thus, we tested whether different formulations affected the EMT-like morphological changes on B16F10 cells after incubation with platelets. After co-cultured with platelets for 24 h, B16F10 cells showed obvious EMT-like morphological changes, which altered from polygon to spindle (Figure 3D). The mesenchymal-like cells were easier to invade and metastasize [22]. On the contrary, free LMWH- or LMWH/PPD-treated cells showed a similar morphology like HEPES-treated group, which was almost the initial morphology and only several cells showed the trend to stretch. In comparison, PPD-treated and free DOX-treated groups all exhibited EMT-like morphological changes like HEPES + platelets-treated group.

Western blot of E-cadherin and N-cadherin

To explore the anti-metastatic mechanisms of LMWH, markers involved in EMT (e.g. E-cadherin and N-cadherin) were detected by western blot. E-cadherin was a member of the Ca^{2+}-dependent integral membrane cell-cell adhesion receptor family and was localized at the zonula adherens junction between epithelial cells [40, 41]. Importantly, E-cadherin played an important role in the contacts between tumor cells and the loss of it might promote the early step of tumor metastasis, while N-cadherin possessed the opposite function. As shown in Figure 3E, 3F and 3G (3F and 3G were the semi-quantitative results), the expression level of E-cadherin was significantly reduced in HEPES + platelet-treated group when compared with HEPES-treated group. However, the expression level of the mesenchymal cell-cell adhesion related N-cadherin in B16F10 cells was significantly increased after treated with platelets. Free LMWH- and LMWH/PPD-treated group did not show obvious loss of E-cadherin or obvious increase of N-cadherin. However, the levels of E-cadherin or N-cadherin in other groups were significantly changed. These results reflected the regulatory effects of LMWH on the EMT-like transformation process of B16F10 cells. Taken together, the anti-metastatic effects of LMWH on B16F10 cells were confirmed.

In vivo imaging and tissue distribution

Firstly, *in vivo* imaging system was used to evaluate the distribution of different Cy5-DNA-loaded formulations *in vivo*. At the predetermined time points of 30 min, 1 h and 3 h, free DOX+Cy5-DNA group showed little accumulation of Cy5-DNA (Figure 4A) because the distribution of free drug *in vivo* was always nonspecific. In contrast, PPD/Cy5-DNA group showed higher tumor accumulation than free DOX+Cy5-DNA group. And LMWH/PPD/Cy5-DNA group showed higher fluorescence intensity than PPD/Cy5-DNA group, probably because that the positive-charged PPD/Cy5-DNA was more likely to be eliminated by RES. The semi-quantitative results shown in Figure 4B were consistent with the *in vivo* results. The image of the isolated organs (3 h) was shown in Figure 4C, suggesting that the Cy5-DNA was mainly eliminated by kidney. Moreover, *ex vivo* imaging of the tumors (3 h) clearly indicated that the fluorescence intensity of LMWH/PPD/Cy5-DNA was stronger than the other two formulations (Figure 4C), which was consistent with the *in vivo* imaging results.

Furthermore, the frozen sections of tumors were observed by laser scanning confocal microscope. As shown in Figure 4D, all groups showed fluorescence distribution around the edges of tumors, among which LMWH/PPD/Cy5-DNA group showed the strongest fluorescence. Besides, LMWH/PPD/Cy5-DNA also showed strong fluorescence in the center of tumors (Figure 4E), mainly because small-sized LMWH/PPD/Cy5-DNA was easy to penetrate in the tumor sites. PPD/Cy5-DNA also showed fluorescence distribution in the center of tumors, which was weaker than that of LMWH/PPD/Cy5-DNA, probably because PPD delivered less Cy5-DNA into the tumor sites. Free DOX+Cy5-DNA showed negligible fluorescence distribution in the center of

tumors. These biodistribution studies clearly indicated that LMWH/PPD can significantly enhance tumor accumulation of nucleic acid drugs *in vivo*.
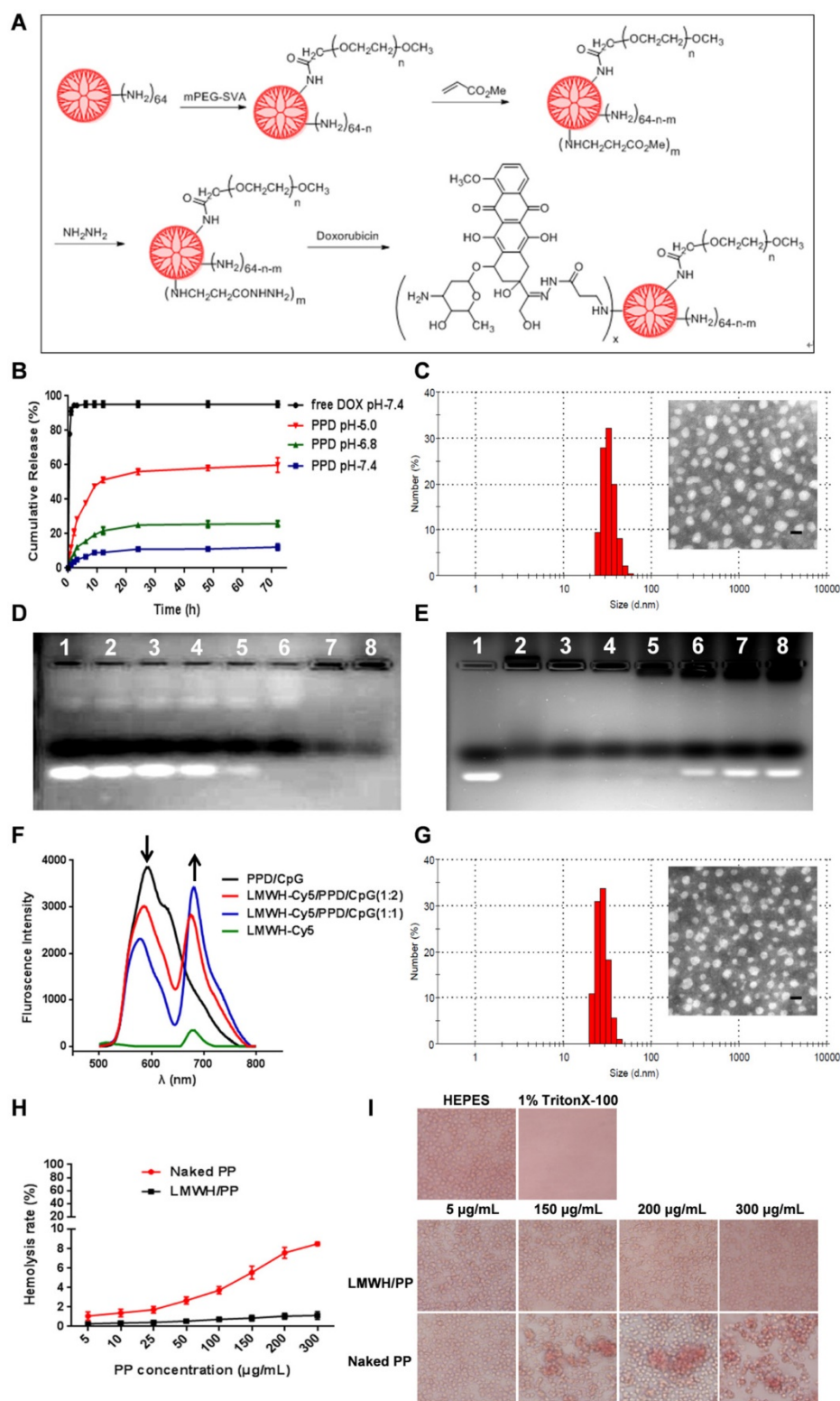

Figure 2. (A) Schematic illustration of reaction scheme for the synthesis of PPD conjugates. (B) Cumulative released DOX from PPD in pH 7.4, 6.8 and 5.0 at different time points. (C) DLS and TEM image of PPD, The scale bar represents 50 nm. (D) CpG ODNs condensation ability of PPD. Lane 1 represents naked CpG ODNs. The mass ratios of PPD to CpG ODNs in lane 2-7 are: 0.2: 1, 0.5: 1, 1: 1, 2: 1, 4: 1, 8: 1, 12: 1. (E) Amount of LMWH determined by agarose gel electrophoresis. Group1 represents Naked CpG ODNs and the mass ratios of LMWH to PPD in lane 2-7 are: 0.1: 1, 0.25: 1, 0.4: 1, 0.6: 1, 0.8: 1, 1.0: 1, 1.2: 1. (F) Fluorescence emission spectra of various formulations with Cy5/DOX mass ratios of 0: 2, 1: 2, 1: 1 and 2: 0. (G) DLS and TEM image of LMWH/PPD/CpG. The scale bar represents 50 nm. (H) Hemolysis rate (%) of red blood cells when treated with different concentrations of PP and LMWH/PP. (I) Images of red blood cells when treated with Naked PP and LMWH/PP at various concentrations.
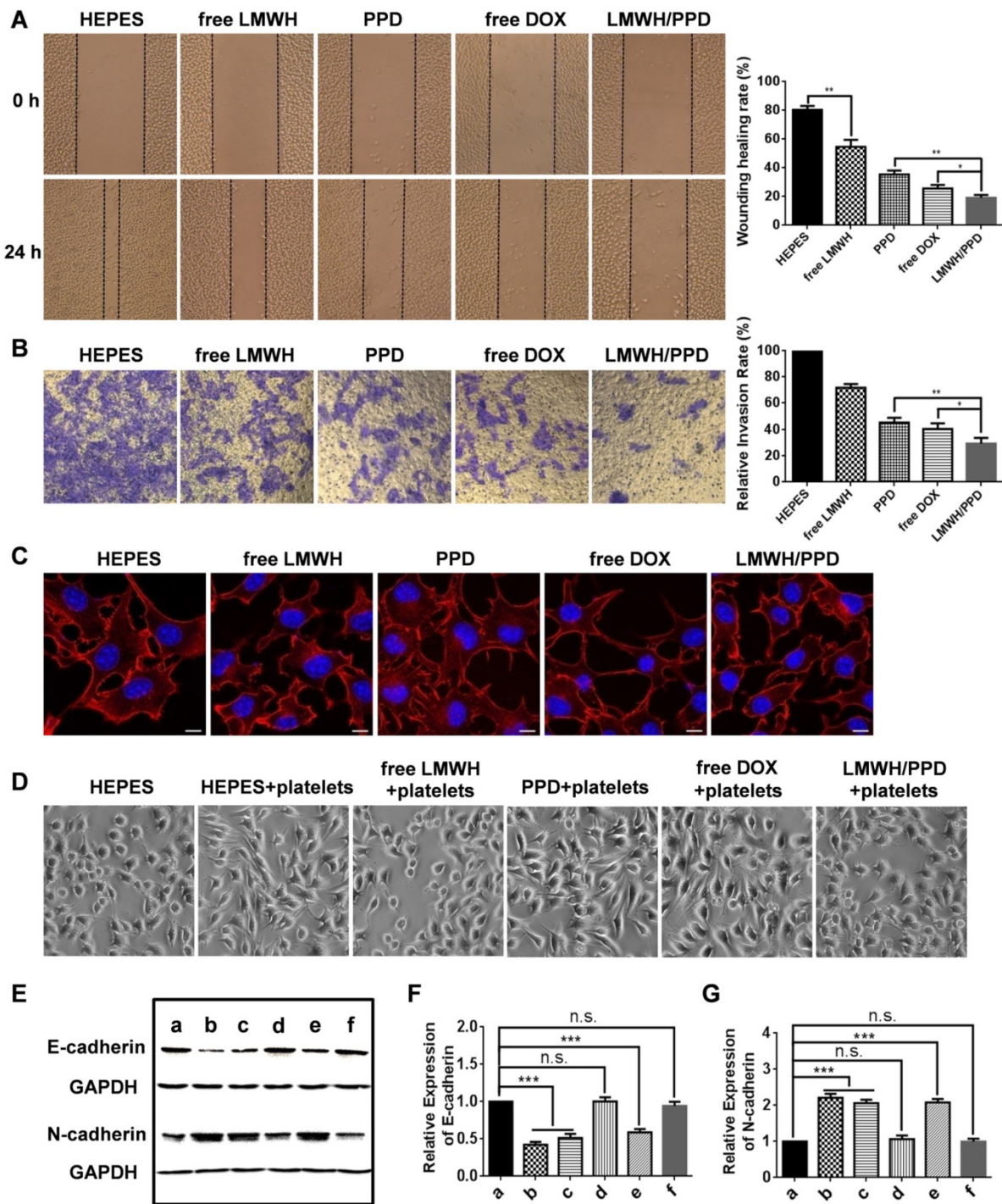
Figure 3. The anti-metastatic effects and mechanisms of LMWH and LMWH/PPD. (A) Images and wound healing rates after incubation with HEPES, free LMWH, PPD, free DOX or LMWH/PPD for 24 h (n = 3, means ± SD). *p < 0.05, **p < 0.01. Images were captured at 0 h and 24 h. (B) Images and quantitative analysis of invaded B16F10 cells after incubation with HEPES, free LMWH, PPD, free DOX, LMWH/PPD for 48 h (n = 3, means ± SD). *p < 0.05, **p < 0.01. (C) Actin cytoskeleton of B16F10 cells after incubation with HEPES, free LMWH, PPD, free DOX or LMWH/PPD. The scale bar represents 10 μm. (D) Images of B16F10 cells after incubation with different formulations. (E) Levels of E-cadherin and N-cadherin detected by western blot. a, HEPES; b, HEPES + platelets; c, free Dox + platelets; d, free LMWH + platelets; e, PPD + platelets; f, LMWH/PPD + platelets. Semi-quantitative levels of (F) E-cadherin and (G) N-cadherin normalized to HEPES group (n = 3, means ± SD). *p < 0.05, **p < 0.01, ***p < 0.001.

In addition, the accumulation of carriers on B16F10 tumor-bearing mice was also investigated. Fluorescent probe Cy7 was conjugated onto PPD by amidation reaction. As shown in Figure S8, LMWH/PPD-Cy7 group showed obvious fluorescence in tumor sites which indicated the accumulation of Cy7-labled nanoparticles and the fluorescence intensity of LMWH/PPD-Cy7 group was stronger than that of PPD-Cy7 group at all time points, which might benefit from the coating of LMWH.

Effects of DOX on CRT exposure and HMGB1 release

Previous reports have indicated that the direct killing of tumor cells mediated by DOX could produce tumor-associated antigens and emit "eating me" signals, such as CRT and HMGB1, which might be involved in the downstream immune responses [11, 42]. The CRT exposure was a crucial mark for ICD, so we detected the capacity of DOX to induce CRT exposure on B16F10 cells by laser scanning confocal microscope and flow cytometry. As shown in Figure 5A, free DOX-treated cells exhibited large amount of CRT exposure as compared with HEPES-treated cells. PPD and LMWH/PPD also

induced obvious CRT exposure but their amounts were slightly lower than that of free DOX group, which might be due to the sustained-release effect of DOX. The results from flow cytometry were consistent with that form the laser scanning confocal microscopy (Figure 5B). In addition, HMGB1 release was another mark for ICD. The CRT exposure and HMGB1 release induced by DOX were assessed by immunohistochemical staining *in vivo*. As shown in Figure 5C, mice treated with LMWH/PPD acquired the maximum CRT exposure and HMGB1 release, which might be due to the enhanced DOX delivery efficiency mediated by LMWH/PPD. In comparison, mice treated with free DOX elicited minimum CRT exposure and HMGB1 release *in vivo*.
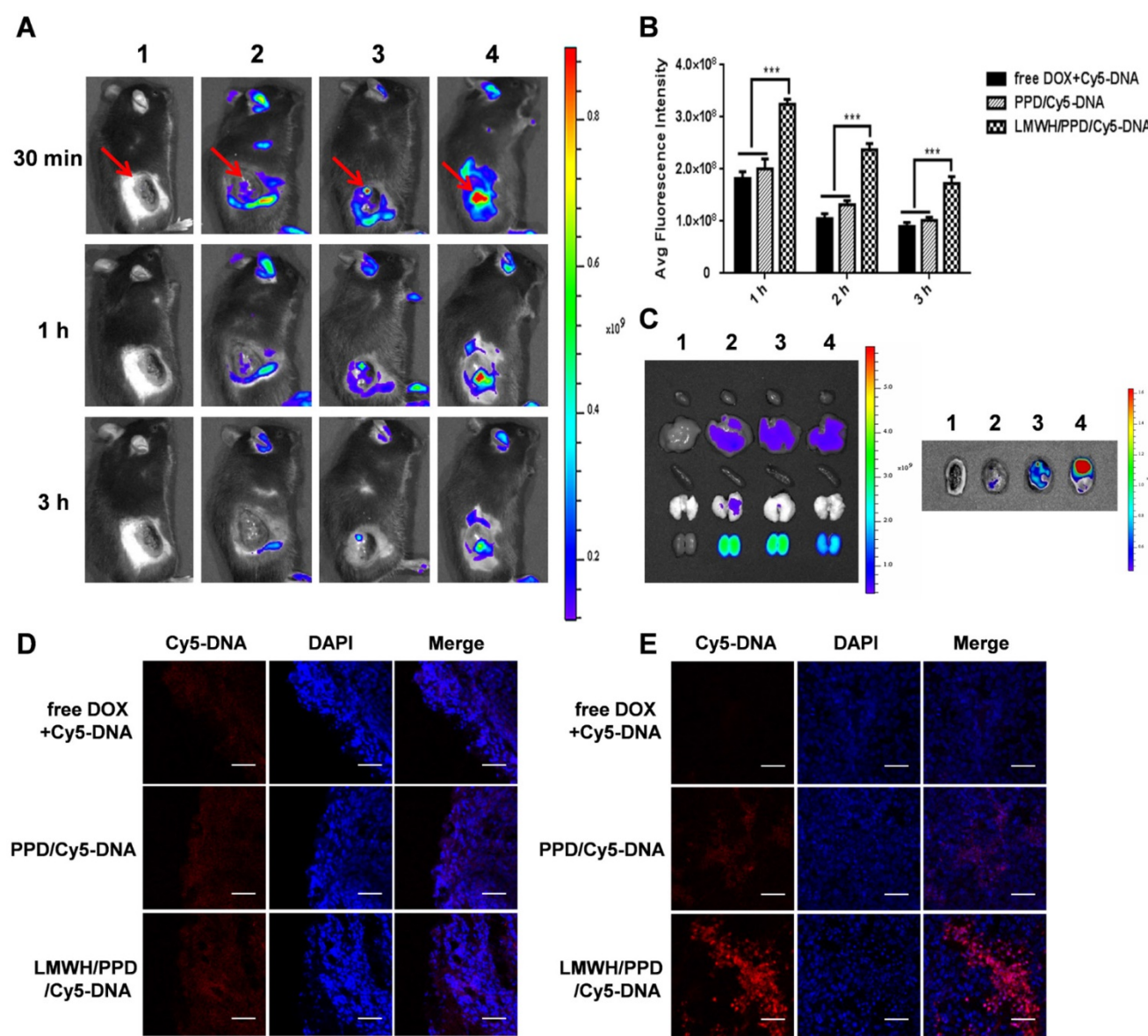

Figure 4. *In vivo* distribution of different formulations. (A) *In vivo* images of B16F10 tumor-bearing mice at 30 min, 1 h and 3 h after systemic administration: 1, HEPES; 2, free DOX+Cy5-DNA; 3, PPD/Cy5-DNA; 4, LMWH/PPD/Cy5-DNA. Red arrows indicate the tumors. (B) The semi-quantitative results of *in vivo* imaging. ***p < 0.001. (C) Photos of isolated organs and tumors. The groups are consistent with (A). The edge (D) and the center (E) of isolated tumors observed by laser scanning confocal microscope. The scale bar represents 50 μm.
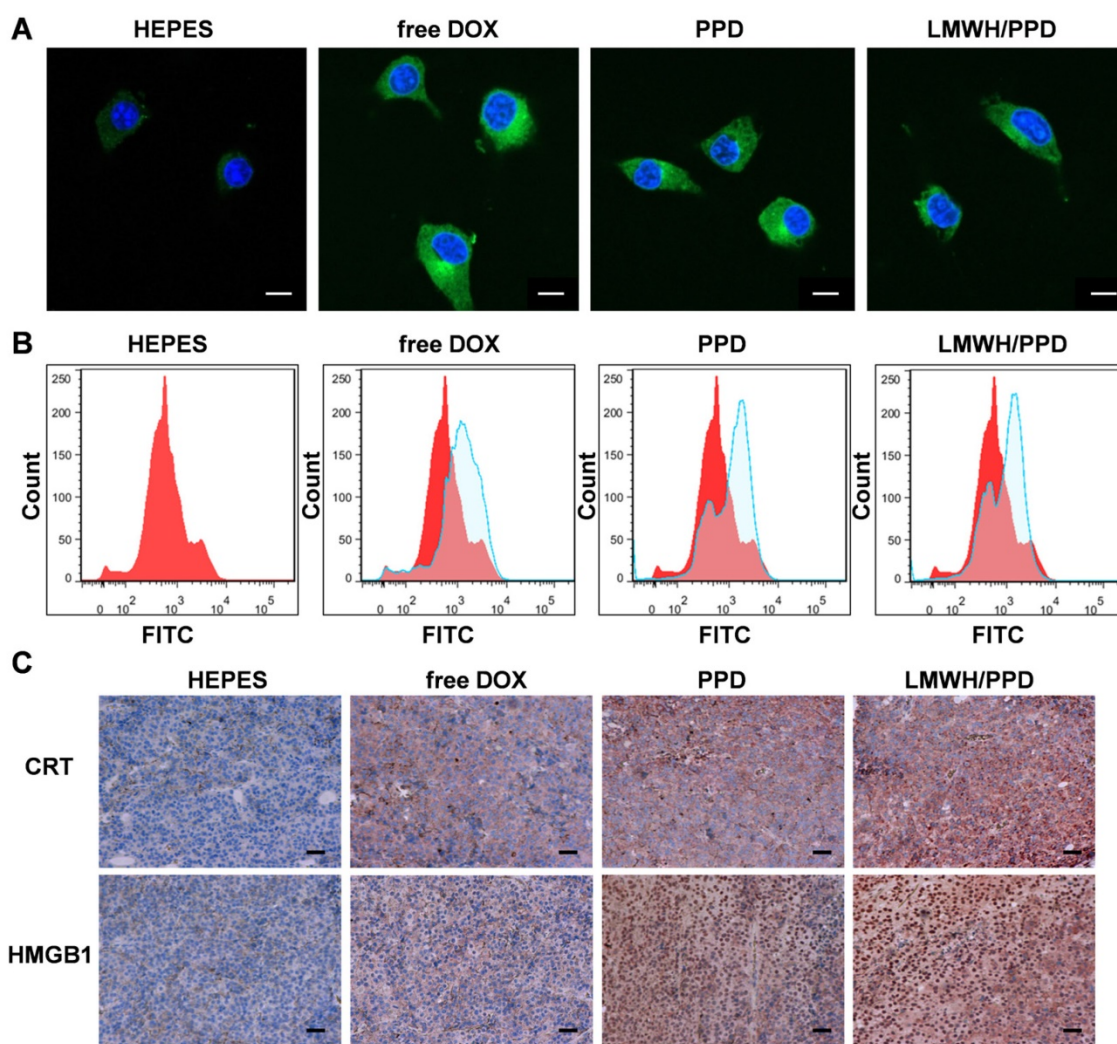
Figure 5. Effects of DOX on CRT exposure and HMGB1 release. (A) Immunofluorescence detection of CRT by laser scanning confocal microscope. The scale bar represents 100 μm. (B) Detection of CRT exposure on B16F10 cells by flow cytometry. (C) Immunohistochemical staining of CRT and HMGB1 in the paraffin sections of tumors (both shown in reddish brown).

LMWH/PPD/CpG realized the optimal immune responses

After capturing and processing the antigens to form MHC-peptide (pMHC) complexes, DCs underwent maturation and up-regulation of the expression of costimulatory molecules (e.g., CD40, CD80 and CD86), which further enhanced the activation of naive T cells and boosted the immune responses [43]. To evaluate the immune status *in vivo*, the draining lymph nodes and tumors of mice were collected and analyzed. Firstly, the maturation of DCs was detected by the markers of CD40, CD80, CD86 on $CD11C^+$ DCs. As shown in Figure 6A, 6B and 6C, treatment with LMWH/PPD/CpG induced the highest percentages of $CD40^+CD11c^+$, $CD80^+CD11c^+$ and $CD86^+CD11c^+$ cells. The maturation rates of DCs in PPD/CpG group were significantly higher than PPD group, which verified the immune activation effects of CpG ODNs and suggested that CpG ODNs

could boost the DOX-elicited immune responses. When compared with PPD/CpG group, the percentages of these three kinds of cells in LMWH/PPD/CpG group were significantly increased (1.22-fold, 1.69-fold and 1.19-fold, respectively). Next, T cells in tumor regions were also analyzed by flow cytometry. The helper T cells ($CD3^+CD4^+$) were responsible for both humoral and cell-mediated immunity, while the cytotoxic T cells ($CD3^+CD8^+$) had a direct killing effect on tumor cells by releasing granules including membrane-lytic materials such as perforin and granzymes. As shown in Figure 7A and 7B, the $CD3^+CD4^+$ T cells and $CD3^+CD8^+$ T cells were also remarkably increased after treatment of LMWH/ PPD/CpG. However, the infiltrating regulatory T cells (T_{reg} cells) could suppress the anti-tumor immunity and were involved in the population of $CD4^+$ effector T cells. The ratios of $CD4^+$ effector T cells ($CD4^+$ T_{eff} cells) to T_{reg} cells in different groups were calculated and shown in Figure S9. HEPES

group exhibited the lowest CD4$^+$ T$_{eff}$/T$_{reg}$ ratio and free LMWH group exhibited similar results. In comparison, LMWH/PPD/CpG group exhibited the highest CD4$^+$ T$_{eff}$/T$_{reg}$ ratio by integrating the regulatory effects of DOX and CpG ODNs.

In addition, the secretion of cytokine in mice blood was detected by ELISA. IFN-γ was a multifunctional cytokine which was primarily secreted by the activated T cells and also played a pivotal role in T-helper cell 1 type (Th 1) immune responses [44]. The level of IFN-γ in sera after treatment with LMWH/PPD/CpG was approximately 4-fold higher than HEPES group, and was also higher than PPD, PPD/CpG or free DOX+CpG group (Figure 7C). These data suggested that LMWH/PPD/CpG could stimulate optimal immunological effects *in vivo*.
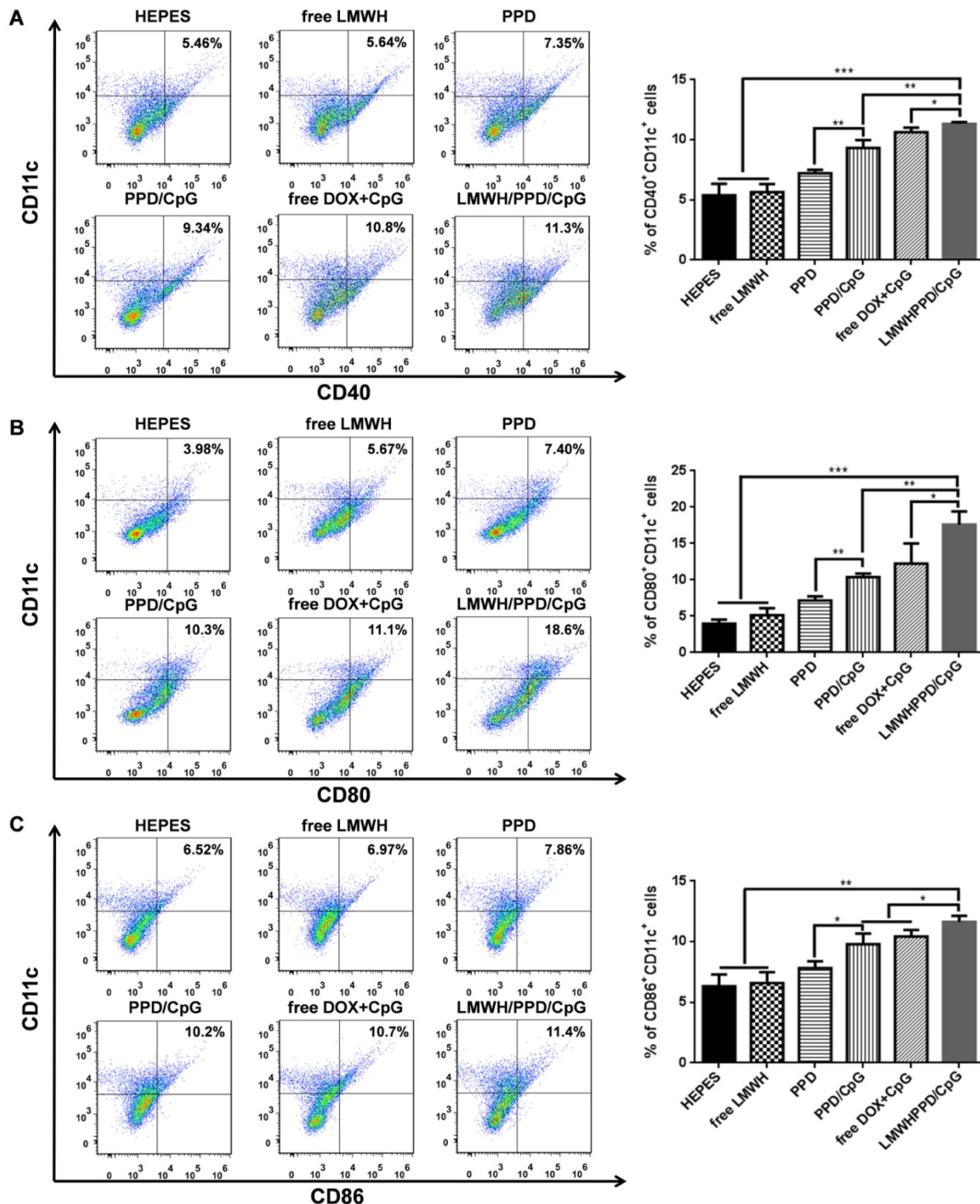

Figure 6. Markers of CD40 (A), CD80 (B) and CD86 (C) expressed on CD11c$^+$ DCs detected by flow cytometry. The graphs respectively reflect the percentages of CD40$^+$CD11c$^+$ cells, CD80$^+$CD11c$^+$ cells and CD86$^+$CD11c$^+$ cells after various treatments. *p < 0.05, **p < 0.01, ***p < 0.001.
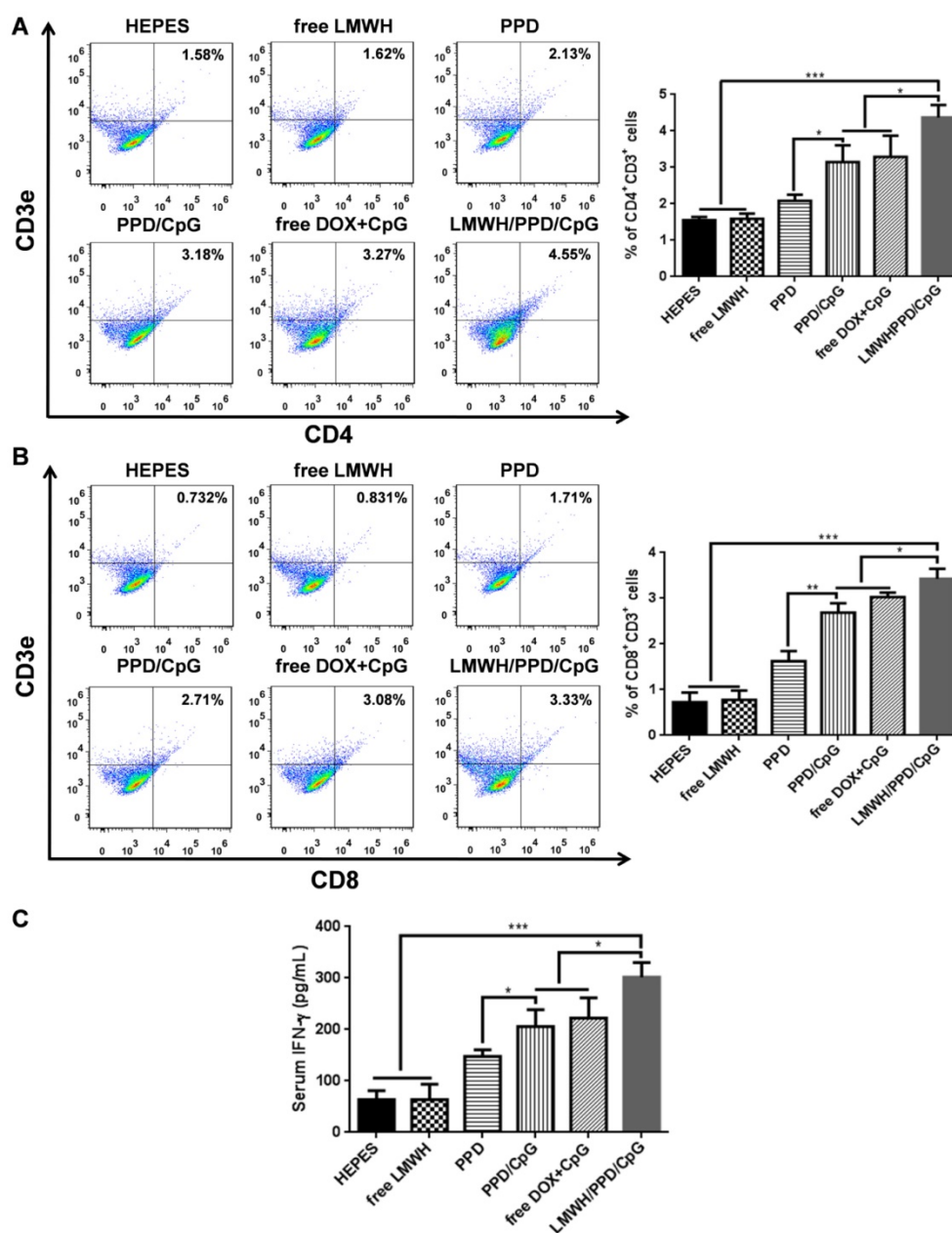
Figure 7. Quantification of CD4+CD3+ cells (A) and CD8+CD3+ cells (B) in tumors by flow cytometry after various treatments. (C) IFN-γ in serum after various treatments detected by ELISA. *p < 0.05, **p < 0.01, ***p < 0.001.

In vivo anti-tumor efficacy

The anti-tumor efficacy of LMWH/PPD/CpG was analyzed on B16F10 tumor-bearing mice. As shown in Figure 8A, free LMWH group showed negligible inhibitory effects on tumor growth and the inhibitory rate of PPD on tumor growth was obviously increased owing to the killing effects of DOX. After the co-delivery of CpG ODNs, PPD/CpG showed a higher inhibitory rate on tumor growth than PPD, which might be attributed to the synergistic effects of DOX and CpG ODNs. Among all groups, LMWH/PPD/CpG presented the strongest anti-tumor efficacy and the tumor volume of LMWH/PPD/CpG group was significantly smaller than that of other groups (Figure 8A and 8B). Individual tumor growth curves of various groups were also presented (Figure 8C). During the whole treatment period, mice treated with free DOX+CpG showed obvious weight loss which might come from the systemic toxicity of free DOX and CpG ODNs (Figure 8D). In comparison, LMWH/PPD/CpG group did not exhibit obvious weight loss, indicating that this nanosystem could reduce the acute toxicity of free drugs. TUNEL and H&E staining of tumors showed similar results as mentioned above (Figure 6E). H&E staining of major organs also revealed the evident cardiotoxicity in free DOX+CpG group , which might be caused by free DOX (Figure 6F).
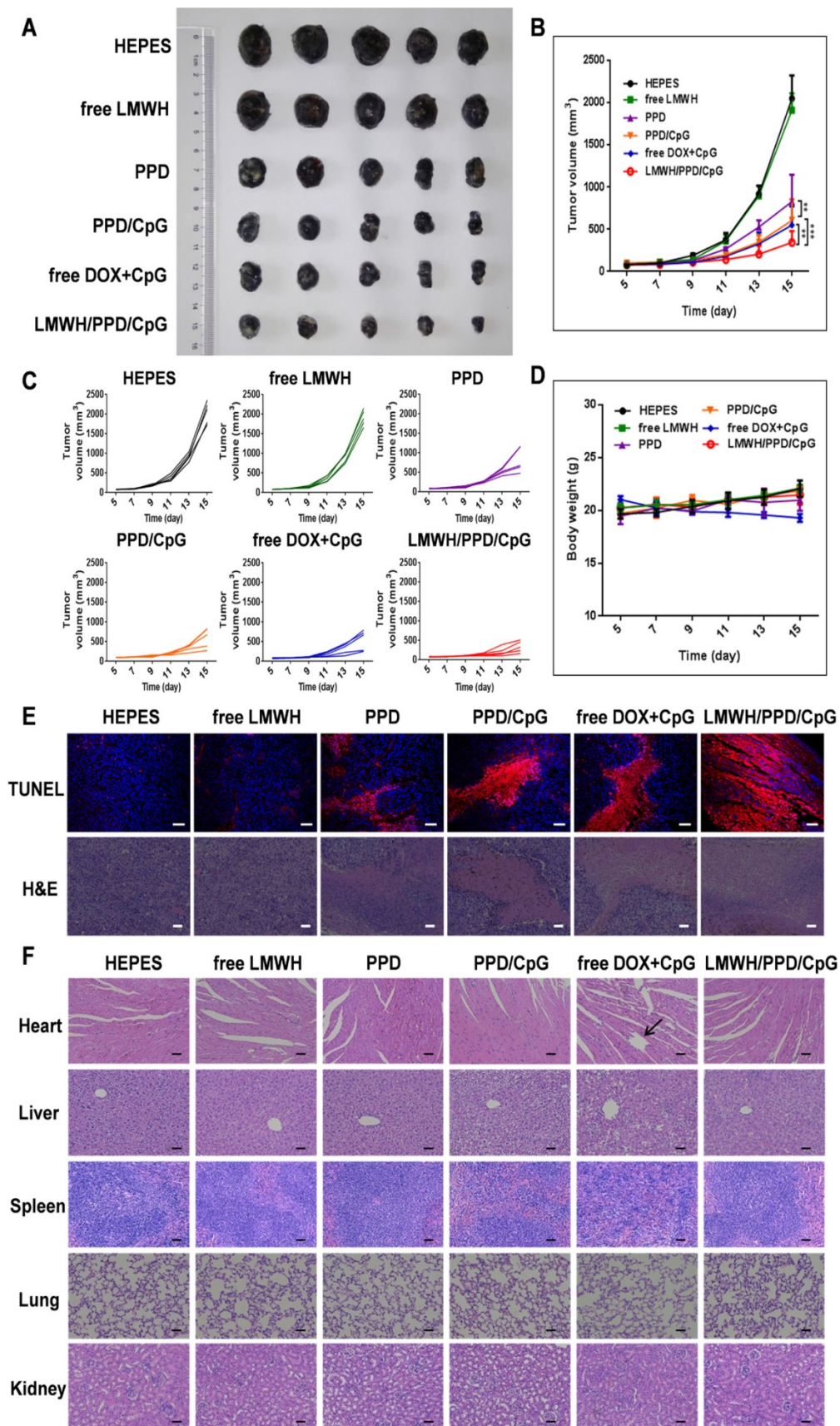
Figure 8. *In vivo* anti-tumour efficacy of indicated formulations. (A) Photographs of tumors at the end of treatments. (B) Tumor growth curves of various groups. *p < 0.05, **p < 0.01, ***p < 0.001. (C) Individual tumor growth curves of various groups. (D) Curves of mice weight changes during the treatment process. (E) TUNEL staining and H&E staining of collected tumors. The scale bar represents 50 μm (TUNEL) or 200 μm (H&E). (F) H&E staining of hearts, livers, spleens, lungs and kidneys in various groups. Black arrow indicates the cardiotoxicity. The scale bar indicates 200 μm.
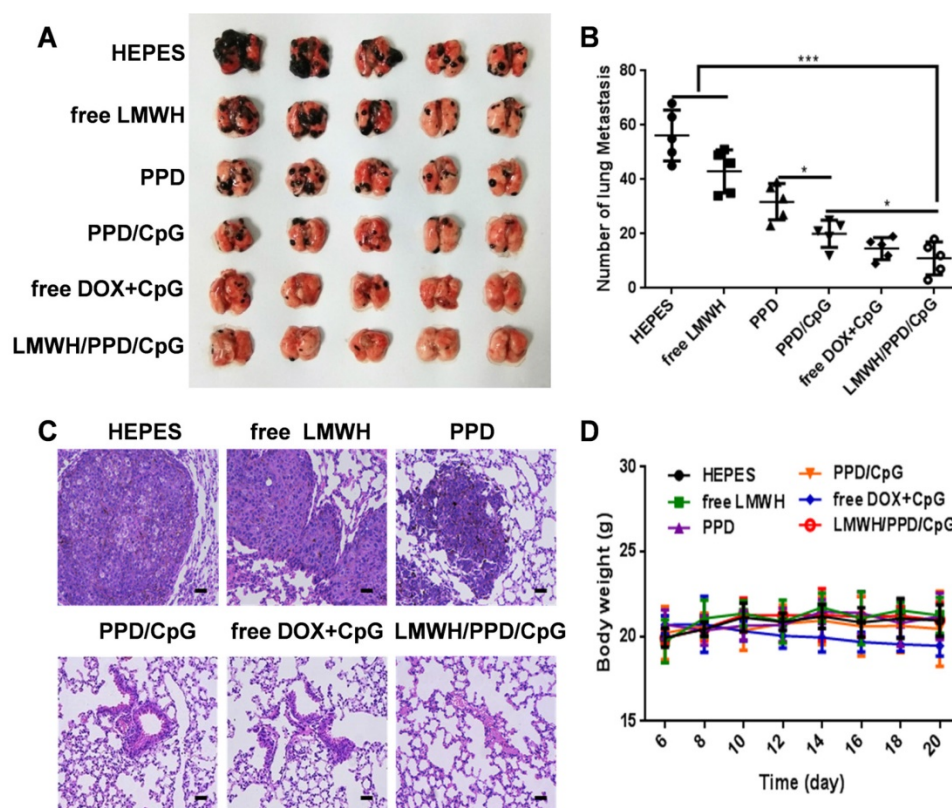
Figure 9. Anti-metastatic effects of the different formulations. (A) Pictures of lung tissues at the end of treatments. (B) Number of lung metastatic nodules in each group. *p < 0.05, **p < 0.01, ***p < 0.001. (C) Histological analysis of lung sections. The scale bar represents 200 μm. (D) Curves of mice body weight changes during the treatment process.

In vivo anti-metastatic efficacy

Whether LMWH/PPD/CpG nanoparticles could inhibit and eradicate B16F10 pulmonary metastasis was another central issue. We assumed that LMWH/PPD/CpG exhibited the anti-metastatic effects by integrating the anti-metastatic abilities of LMWH, the killing effects of DOX and the CpG ODNs enhanced immune activation effects. As shown in Figure 9A and 9B, free LMWH group showed less metastatic nodules when compared with HEPES-treated group, which indicated the anti-metastatic effects of LMWH. LMWH/PPD/CpG exhibited the most effective inhibition on tumor metastasis, thus showed the least pulmonary metastatic nodules. H&E staining was also conducted and exhibited similar results (Figure 9C). The weight changes in mice was monitored and only free DOX+CpG group showed weight loss, which might come from the toxicity of free drugs (Figure 9D). H&E staining of other major organs was shown in Figure S10. All data above showed that LMWH/PPD/CpG could inhibit B16F10 pulmonary metastasis effectively, perhaps owing to the multiple functions of LMWH/PPD/CpG.

Conclusion

In summary, we constructed a novel multifunc-
tional core-shell nanoplatform for the combination of immunotherapy and chemotherapy, in which the hydrophilic low molecular weight heparin (LMWH) was used as a part of the carriers to shield the positive charge of nanocore and also to provide favorable anti-metastatic effects. Owing to the coating of LMWH, the negative-charged LMWH/PPD/CpG showed enhanced accumulation at tumor sites, improving the delivery efficiency of DOX and CpG ODNs. DOX was able to trigger tumor-specific immunological effects by eliciting ICD. With the help of immunoadjuvant CpG ODNs, the immune status of mice was further activated, exhibiting enhanced maturation of DCs and increased level of specific CTLs *in vivo*. This strategy of combining immunotherapy and chemotherapy on the anti-metastatic nanoplatform showed improved treatment outcome on B16F10 melanoma and could also be used to treat other highly aggressive tumors.

Abbreviations

LMWH: low molecular weight heparin; CpG ODNs: cytosine-phosphate-guanine oligonucleotides; DOX: doxorubicin; ICD: immunogenic cell death; DCs: dendritic cells; CTLs: cytolytic T lymphocytes; CRT: calreticulin; IFN-γ: interferon-γ; RES: reticuloen-

dothelial system; HRMS: high resolution mass spectra; FRET: fluorescence resonance energy transfer; MTT: methylthiazolyldiphenyl-tetrazolium bromide; EMT: epithelial-mesenchymal transition; HMGB1: high-mobility group box 1.

Supplementary Material

Supplementary figures.
http://www.thno.org/v09p0337s1.pdf

Acknowledgments

Competing Interests

The authors have declared that no competing interest exists.

References

[1] Gupta GP, Massagué J. Cancer Metastasis: Building a Framework. Cell. 2006; 127: 679-695.

[2] Fischer KR, Durrans A, Lee S, Sheng J, Li F, Wong ST, et al. Epithelial-to-mesenchymal transition is not required for lung metastasis but contributes to chemoresistance. Nature. 2015; 527: 472-476.

[3] Fidler IJ. Critical determinants of metastasis. Semin Cancer Biol. 2002; 12: 89-96.

[4] Torchilin V. Tumor delivery of macromolecular drugs based on the EPR effect. Adv Drug Deliv Rev. 2011; 63: 131-135.

[5] Scheper RJ, Bulte JW, Brakkee JG, Quak JJ, Schoot E, Balm AJ, et al. Monoclonal antibody JSB-1 detects a highly conserved epitope on the P-glycoprotein associated with multi-drug-resistance. Int J Cancer. 1988; 42: 389-394.

[6] Vanneman M, Dranoff G. Combining Immunotherapy and Targeted Therapies in Cancer Treatment. Nat Rev Cancer. 2012; 12: 237-251.

[7] Yarchoan M, Johnson III BA, Lutz ER, Laheru DA, Jaffee EM. Targeting neoantigens to augment antitumour immunity. Nat Rev Cancer. 2017; 17: 209-222.

[8] Hung CF, Tsai YC, He L, Wu TC. Control of mesothelin-expressing ovarian cancer using adoptive transfer of mesothelin peptide-specific CD8+T cells. Gene Ther. 2007; 14: 921-929.

[9] Galluzzi L, Buqué A, Kepp O, Zitvogel L, Kroemer G. Immunological Effects of Conventional Chemotherapy and Targeted Anticancer Agents. Cancer Cell. 2015; 28: 690-714.

[10] Vincent J, Mignot G, Chalmin F, Ladoire S, Bruchard M, Chevriaux A, et al. 5-Fluorouracil Selectively Kills Tumor-Associated Myeloid-Derived Suppressor Cells Resulting in Enhanced T Cell–Dependent Antitumor Immunity. Cancer Res. 2010; 70: 3052-3061.

[11] Kroemer G, Galluzzi L, Kepp O, Zitvogel L. Immunogenic cell death in cancer therapy. Annu Rev Immunol. 2013; 31: 51-72.

[12] Obeid M, Tesniere A, Ghiringhelli F, Fimia GM, Apetoh L, Perfettini JL, et al. Calreticulin exposure dictates the immunogenicity of cancer cell death. Nat Med. 2007; 13: 54-61.

[13] Liu Q, Zhu H, Tiruthani K, Shen L, Chen F, Gao K, et al. Nanoparticle-Mediated Trapping of Wnt Family Member 5A in Tumor Microenvironments Enhances Immunotherapy for B-Raf Proto-Oncogene-Mutant Melanoma. ACS Nano. 2018; 12: 1250-1261.

[14] Duan X, Chan C, Lin W. Nanoparticle-mediated Immunogenic Cell Death Enables and Potentiates Cancer Immunotherapy. Angew Chem. 2018; 10.1002/ange.201804882

[15] Nam GH, Lee EJ, Kim YK, Hong Y, Choi Y, Ryu MJ, et al. Combined Rho-kinase inhibition and immunogenic cell death triggers and propagates immunity against cancer. Nat Commun. 2018; 9: 2165.

[16] Vollmer J, Krieg AM. Immunotherapeutic applications of CpG oligodeoxynucleotide TLR9 agonists. Adv Drug Deliv Rev. 2009; 61: 195-204.

[17] Lan X, Voznyy O, Kiani A, Arquer F, Abbas AS, Kim GH, et al. Passivation Using Molecular Halides Increases Quantum Dot Solar Cell Performance. Adv Mater. 2016; 28: 299-304.

[18] Wei M, Chen N, Li J, Yin M, Liang L, He Y, et al. Polyvalent Immunostimulatory Nanoagents with Self-Assembled CpG Oligonucleotide-Conjugated Gold Nanoparticles. Angew Chem. 2012; 51: 1202-1206

[19] Chaffer CL, Weinberg RA. A Perspective on Cancer Cell Metastasis. Science. 2011; 331: 1559-1564.

[20] Nguyen DX, Bos PD, Massagué J. Metastasis: from dissemination to organ-specific colonization. Nat Rev Cancer. 2009; 9: 274-284.

[21] Valastyan S, Weinberg RA. Tumor Metastasis: Molecular Insights and Evolving Paradigms. Cell. 2011; 147: 275-292.

[22] Labelle M, Begum S, Hynes RO. Direct Signaling between Platelets and Cancer Cells Induces an Epithelial-Mesenchymal-Like Transition and Promotes Metastasis. Cancer Cell. 2011; 20: 576-590.

[23] Pearlstein E, Ambrogio C, Karpatkin S. Effect of antiplatelet antibody on the development of pulmonary metastases following injection of CT26 colon adenocarcinoma, Lewis lung carcinoma, and B16 amelanotic melanoma tumor cells into mice. Cancer Res. 1984; 44: 3884-3887.

[24] Mei L, Liu Y, Xia C, Zhou Y, Zhang Z, He Q. Polymer-drug nanoparticles combine doxorubicin carrier and heparin bioactivity functionalities for primary and metastatic cancer treatment. Mol Pharm. 2017; 14: 513-522.

[25] Komatsu N, Waki M, Sue M, Tokuda C, Kasaoka T, Nakajima M, et al. Heparanase expression in B16 melanoma cells and peripheral blood neutrophils before and after extravasation detected by novel anti-mouse heparanase monoclonal antibodies. J Immunol Methods. 2008; 331: 82-93.

[26] Han HD, Lee A, Song CK, Hwang T, Seong H, Lee CO, et al. In vivo distribution and antitumor activity of heparin-stabilized doxorubicin-loaded liposomes. Int J Pharm. 2006; 313: 181-188.

[27] Zhu S, Hong M, Tang G, Qian L, Lin J, Jiang Y, et al. Partly PEGylated polyamidoamine dendrimer for tumor-selective targeting of doxorubicin: the effects of PEGylation degree and drug conjugation style. Biomaterials. 2010; 31: 1360-1371.

[28] Tomalia DA, Baker H, Dewald J, Hall M, Kallos G, Martin S, et al. A New Class of Polymers: Starburst-Dendritic Macromolecules. Polymer J. 1985; 17: 117-132.

[29] Wu HM, Pan SR, Chen MW, Wu Y, Wang C, Wen YT, et al. A serum-resistant polyamidoamine-based polypeptide dendrimer for gene transfection. Biomaterials. 2011; 32: 1619-1634.

[30] Chen KJ, Chiu YL, Chen YM, Ho YC, Sung HW. Intracellularly monitoring/ imaging the release of doxorubicin from pH-responsive nanoparticles using Förster resonance energy transfer. Biomaterials. 2011; 32: 2586-2592.

[31] Kneidl B, Peller M, Winter G, Lindner LH, Hossann M. Thermosensitive liposomal drug delivery systems: state of the art review. Int J Nanomedicine. 2014; 9: 4387-4398.

[32] Jares-Erijman EA, Jovin TM. FRET imaging. Nat Biotechnol. 2003; 21: 1387-1395.

[33] Lv Y, Xu C, Zhao X, Lin C, Yang X, Xin X, et al. Nanoplatform Assembled from a CD44-Targeted Prodrug and Smart Liposomes for Dual Targeting of Tumor Microenvironment and Cancer Cells. ACS Nano. 2018; 12: 1519-1536.

[34] Noh SM, Park MO, Shim G, Han SE, Lee HY, Huh JH, et al. Pegylated poly-l-arginine derivatives of chitosan for effective delivery of siRNA. J Control Release. 2010; 145: 159-164.

[35] Mei L, Liu Y, Zhang H, Zhang Z, Gao H, He Q. Antitumor and Antimetastasis Activities of Heparin-based Micelle Served As Both Carrier and Drug. ACS Appl Mater Interfaces. 2016; 8: 9577–9589

[36] Kramer N, Walzla A, Unger C, Rosnera M, Krupitza G, Hengstschläger M, et al. In vitro cell migration and invasion assays. Mutat Res Rev Mutat Res. 2013; 752: 10–24.

[37] Geiger T, Geiger B. Towards elucidation of functional molecular signatures of the adhesive-migratory phenotype of malignant cells. Semin. Cancer Biol. 2010; 20: 146-152.

[38] Chalkiadaki G, Nikitovic D, Katonis P, Berdiaki A, Tsatsakis A, Kotsikogianni I, et al. Low molecular weight heparin inhibits melanoma cell adhesion and migration through a PKCa/JNK signaling pathway inducing actin cytoskeleton changes. Cancer Lett. 2011; 312: 235-244.

[39] Yamaguchi H, Condeelis J. Regulation of the actin cytoskeleton in cancer cell migration and invasion. Biochim Biophys Acta Mol Cell Res. 2007; 1773: 642-652.

[40] Rajasekaran AK, Hojo M, Huima T, Rodriguez-Boulan E. Catenins and zonula occludens-1 form a complex during early stages in the assembly of tight junctions. J Cell Biol. 1996; 132: 451-463.

[41] Takeichi M. Morphogenetic roles of classic cadherins. Curr Opin Cell Biol.1995; 7: 619-627.

[42] Fridlender ZG, Sun J, Singhal S, Kapoor V, Cheng G, Suzuki E, et al. Chemotherapy delivered after viral immunogene therapy augments antitumor efficacy via multiple immune-mediated mechanisms. Mol Ther. 2010; 18: 1947-1959.

[43] Akira S, Takeda K, Kaisho T. Toll-like receptors : critical proteins linking innate and acquired immunity. Nat Immunol. 2001; 2: 675-680.

[44] Cao Y, Ma Y, Zhang M, Wang H, Tu X, Shen H, et al. Ultrasmall Graphene Oxide Supported Gold Nanoparticles as Adjuvants Improve Humoral and Cellular Immunity in Mice. Adv Funct Mater. 2014; 24: 6963–6971